

Challenges in calculations for multi-particle processes*

A. van Hameren

Institut für Physik, Johannes-Gutenberg-Universität, Mainz, Germany

C.G. Papadopoulos

Institute of Nuclear Physics, NCSR “Demokritos”, 15310 Athens, Greece

November 25, 2018

Abstract

The physics of high-energy collider experiments asks for delicate comparisons between theoretical predictions and experimental data. Signals and potential backgrounds for new physics have to be predicted at sufficient accuracy. The accuracy as well as the computational complexity of the calculations leading to the predictions depend on both the number of external particles in the process analyzed and the order of the quantum corrections, the number of loops, included in the calculation. We present some approaches to problems occurring in these calculations regarding the integration of phase-space and the inclusion of one-loop corrections.

1 Introduction

Collider experiments played and continue to play a fundamental rôle in particle physics. This is exemplified by past, current and future experiments like, *e.g.* LEP at CERN, Tevatron at Fermilab or HERA at DESY, and LHC, again at CERN, respectively. Current research focuses on even more precise tests of what is known as the Standard Model of particle physics, the validity of which needs the discovery of the Higgs boson at such a collider experiment. This asks for new colliders to reach higher energies leading to events from scattering experiments with higher numbers of particles involved.

In order to prepare and analyze the outcome of the experiments, signals and potential backgrounds for new physics have to be predicted at sufficient accuracy.

*Presented at the final meeting of the European Network “Physics at Colliders”, Montpellier, September 26-27, 2004.

Most of the calculations involved are set up within the framework of perturbation theory, in which the accuracy is controlled by the order parameter. In the application to quantum field theory, on which the Standard Model is based, the order parameter is connected to both the number of external particles in the process analyzed and the order of the quantum corrections, the number of loops, included in the calculation.

The Standard Model is tested mainly by the comparison of the experimental data and theoretical calculations on the statistical level. This can happen through the analysis of cross sections, or simulation of collider experiments. Both the increase in the multiplicity of particles at the experiments, and the need for higher accuracy of theoretical calculations lead to a dramatic increase of the complexity of this analysis. In the following, we will encounter two particular examples in which this increase of complexity constitutes a challenge in the scientific process.

2 A hierarchical phase space generator for QCD antennas

The reliable description of multi-jet production at collider experiments is an important issue in the study of the Standard Model. It requires the calculation of cross sections, which again requires the integration of squared scattering amplitudes over phase space. The number of dimensions of the integration space in combination with the desired cuts point at the Monte Carlo method as the only suitable candidate for this task. Since the computation of QCD scattering matrix elements with many particles is rather time-consuming, the integration process should preferably involve as few integration points as possible. The strong peaking structures exhibited in the QCD amplitudes enforce the application of the Monte Carlo method to be dressed with a sophisticated portion of importance sampling. Flat phase space generators, like **RAMBO** [1], will not be adequate for this task.

In the last years several methods to efficiently integrate the peaking structures of the scattering amplitudes have emerged, and have been used in several contexts [2]. For instance, **PHEGAS** [3] is an example where an efficient, automated, mapping of all possible peaking structures of a given scattering process has been established. The algorithm is based on the “natural” mappings dictated by the Feynman graphs contributing to the given process, so that the number of kinematic channels used to generate the phase space is equal to the number of Feynman graphs. Using adaptive methods, like multi-channel optimization [4] and by throwing away channels that are negligible, we may end up with a few channel generator exhibiting high efficiency, as is indeed the case in $n(+\gamma)$ -fermion production in e^+e^- collisions. In contrast, the QCD scattering amplitudes point towards the opposite direction: large number of Feynman graphs which means

large number of kinematic channels which, moreover, contribute equally to the result.

A way out off this problem may be based on the long-standing remark that $n + 2$ -gluon amplitude may be described by a very compact expression when special helicities are assigned to the gluons, which, combined with the leading color approximation, results to

$$\sum_c |\mathcal{M}|^2 = 8 \left(\frac{N_c}{2} \right)^n (N_c^2 - 1) \sum_{1 \leq i < j}^{n+2} (p_i \cdot p_j)^4 \sum_{P(2, \dots, n+2)} A_{n+2}(p_1, \dots, p_{n+2}) , \quad (1)$$

where N_c refers to the number of colors,

$$A_{n+2}(p_1, \dots, p_{n+2}) = [(p_1 \cdot p_2)(p_2 \cdot p_3) \cdots (p_{n+1} \cdot p_{n+2})(p_{n+2} \cdot p_1)]^{-1} , \quad (2)$$

and the sum over all permutations of the 2^{nd} to the $(n + 2)^{\text{nd}}$ argument of this function is taken, with the exception of those that are equivalent under reflection $i \mapsto n + 4 - i$ [5].

SARGE [6] is the first known example of a phase space generator that deals with the momentum structures entering the above expression, namely with (2), known as *antenna structures*. The algorithm is based on the “democratic” strategy to generate the n body phase space, as is the case for **RAMBO**, and it makes use of the scale symmetry of the antenna to achieve the required goal. Now, we study the “hierarchical” strategy for phase space generation in order to efficiently map the momentum antenna structures. The idea is as follows. Using the standard two-body phase space (neglecting factors of 2π)

$$d\Phi_2(P; s_1, s_2; p_1, p_2) = d^4 p_1 \delta_+(p_1^2 - s_1) d^4 p_2 \delta_+(p_2^2 - s_2) \delta^4(P - p_1 - p_2) , \quad (3)$$

we decompose the phase space

$$d\Phi_n(P; p_1 \dots, p_n) = \delta^4\left(\sum_{i=1}^n p_i - P\right) \prod_{i=1}^n d^4 p_i \delta_+(p_i^2 - \sigma_i) \quad (4)$$

as

$$\begin{aligned} d\Phi_n(P; p_1 \dots, p_n) &= ds_{n-1} d\Phi_2(Q_n; \sigma_n, s_{n-1}; p_n, Q_{n-1}) \\ &\times ds_{n-2} d\Phi_2(Q_{n-1}; \sigma_{n-1}, s_{n-2}; p_{n-1}, Q_{n-2}) \\ &\vdots \\ &\times ds_2 d\Phi_2(Q_3; \sigma_3, s_2; p_3, Q_2) \\ &\times d\Phi_2(Q_2; \sigma_2, \sigma_1; p_2, p_1) . \end{aligned} \quad (5)$$

The task is to express the phase space in terms of the invariants $p_i \cdot p_j$ appearing in the antenna structure (2), so that, using a suitable mapping, we can construct a density that, apart from constant and soft terms, will be identical to this antenna structure.

2.1 Antenna generation

In this section, we will present a sketch of how the antenna structures can be generated using the hierarchical approach. For a treatment in full detail, we refer to [7]. The starting point is the generation of the two-body phase space (3) in terms of the variables

$$a_1 = \frac{q_1 \cdot p_1}{q_1 \cdot P} \quad , \quad a_2 = \frac{p_2 \cdot q_2}{P \cdot q_2} \quad , \quad (6)$$

where q_1, q_2 are given massless momenta. Let us introduce the notation

$$c = \cos(\angle(\vec{q}_1, \vec{q}_2)) \quad , \quad s = \sqrt{1 - c^2} \quad (7)$$

and

$$s = P^2 \quad , \quad \bar{s}_{1,2} = s_{1,2}/s \quad . \quad (8)$$

We find that the parameterization

$$\begin{aligned} p_1^0 &\leftarrow (s + s_1 - s_2)/(2\sqrt{s}) \quad , \\ p_1^3 &\leftarrow p_1^0 - \sqrt{s} a_1 \quad , \\ p_1^2 &\leftarrow ((\sqrt{s} - p_1^0 - \sqrt{s} a_2) + c p_1^3)/s \quad , \\ p_1^1 &\leftarrow \pm((p_1^0)^2 - s_1 - (p_1^2)^2 - (p_1^3)^2)^{1/2} \quad , \end{aligned} \quad (9)$$

leads to the identity

$$d\Phi_2(P; s_1, s_2; p_1, p_2) = da_1 da_2 \Pi(a_1, a_2)^{-1/2} \Theta(\Pi(a_1, a_2)) \quad , \quad (10)$$

where

$$\begin{aligned} \Pi(a_1, a_2) &= 4s^2[(1 - a_2 + \bar{s}_2 - \bar{s}_1)a_2 - \bar{s}_2] \\ &- [(1 - 2a_1 - \bar{s}_1 + \bar{s}_2) + (1 - 2a_2 - \bar{s}_1 + \bar{s}_2)c]^2 \quad , \end{aligned} \quad (11)$$

and Θ is the step function. So in order to obtain a two-body phase space with a density which depends on the invariants a_1, a_2 following some given function $f(a_1, a_2)$, one has to generate a_1, a_2 following a density proportional to $f(a_1, a_2) \times \Pi(a_1, a_2)^{-1/2}$ in the region where $\Pi(a_1, a_2) > 0$, and construct the momenta as given above.

The generation strategy proceeds through a sequence of two-body phase space generations following the decomposition (5). At each two-body generation, one final-state momentum p_k is generated, together with the sum Q_{k-1} of the remaining final-state momenta to be generated. This suggests to label the momenta in a way opposite to the order of generation, so first p_n, Q_{n-1} are generated, then p_{n-1}, Q_{n-2} and so on. The starting point is the center of mass frame (CMF) of the initial momenta q_1 and q_2 with $Q_n = q_1 + q_2$ being the overall momentum. The CMF of momentum Q_k we denote by CMF_k . The pair p_k, Q_{k-1} is generated by

generating variables $a_1^{(k)}, a_2^{(k)}$ and constructing the momenta as described before. These variables are now equal to

$$a_1^{(k)} = \frac{p_{k+1} \cdot p_k}{p_{k+1} \cdot Q_k} \quad \text{and} \quad a_2^{(k)} = \frac{q_2 \cdot Q_{k-1}}{q_2 \cdot Q_k} . \quad (12)$$

This happens in CMF_k , so in order to obtain p_k, Q_{k-1} , the constructed momenta have to be boosted such that $(\sqrt{Q_k^2}, 0, 0, 0)$ is transformed to Q_k . Now, we do three observations. Firstly, we have

$$p_{k+1} \cdot Q_k = (Q_{k+1}^2 - Q_k^2 - p_{k+1}^2)/2 . \quad (13)$$

Secondly, we have, with $\Sigma_k = \sum_{i=1}^k \sigma_i$,

$$\frac{s_k - \Sigma_k}{(s_k - \sigma_k - s_{k-1})(s_{k-1} - \Sigma_{k-1})} = \frac{d}{ds_{k-1}} \log \left(\frac{s_{k-1} - \Sigma_{k-1}}{s_k - \sigma_k - s_{k-1}} \right) , \quad (14)$$

and thirdly, we can write

$$\begin{aligned} A_{n+2}(q_1, p_n, p_{n-1} \dots, p_1, q_2) &= \frac{1}{2^{n-1}} (s_n - \Sigma_n) (q_1 \cdot Q_n) (q_2 \cdot Q_n) \\ &\times \left(\prod_{k=n}^3 g_k(s_{k-1}) \frac{1}{a_1^{(k)} a_2^{(k)}} \right) \frac{1}{a_1^{(2)} a_2^{(2)}} , \end{aligned} \quad (15)$$

where $g_k(s_{k-1})$ is given by (14), and where $s_n = Q_n^2$, $p_{n+1} = q_1$ and $Q_1 = p_1$. These observations suggest that the phase space generation

$$\begin{aligned} &ds_{n-1} g_n(s_{n-1}) da_1^{(n)} \frac{1}{a_1^{(n)}} da_2^{(n)} \frac{1}{a_2^{(n)}} \Pi_{(n)}^{-1/2} \Theta(\Pi_{(n)}) \\ &ds_{n-2} g_{n-1}(s_{n-2}) da_1^{(n-1)} \frac{1}{a_1^{(n-1)}} da_2^{(n-1)} \frac{1}{a_2^{(n-1)}} \Pi_{(n-1)}^{-1/2} \Theta(\Pi_{(n-1)}) \\ &\vdots \\ &ds_2 g_3(s_2) da_1^{(3)} \frac{1}{a_1^{(3)}} da_2^{(3)} \frac{1}{a_2^{(3)}} \Pi_{(3)}^{-1/2} \Theta(\Pi_{(3)}) \\ &da_1^{(2)} \frac{1}{a_1^{(2)}} da_2^{(2)} \frac{1}{a_2^{(2)}} \Pi_{(2)}^{-1/2} \Theta(\Pi_{(2)}) , \end{aligned} \quad (16)$$

will lead to a density for the momenta that is proportional to A_{n+2} . Three variables are generated in each CMF_k , namely s_{k-1} , $a_1^{(k)}$ and $a_2^{(k)}$. Just as the integration of s_{k-1} (14), also the integration of $a_1^{(k)}, a_2^{(k)}$ results in a volume factor that depends on the corresponding variables generated in CMF_{k+1} . However, these factors are logarithmic functions of their arguments and exhibit a non-singular behavior, and we call them *soft* factors. The total actual density will

therefore be the product of $n - 1$ soft factors times the antenna structure under consideration.

In the end, we want to generate all permutations in the momenta of (15). Those for which q_1 and q_2 each appear in two factors (none of which is $q_1 \cdot q_2$) cannot be obtained by simple re-labeling. In order to obtain these, we observe that they can be decomposed into two antennas, namely

$$A_{m+2}(q_1, p_m, \dots, p_1, q_2) \times A_{n-m+2}(q_2, p_n, \dots, p_{m+1}, q_1) \quad (17)$$

and each of these can be generated after the decomposition,

$$\begin{aligned} d\Phi_n(P; p_1 \dots, p_n) &= ds_m ds_{n-m} d\Phi_2(Q_n; s_m, s_{n-m}; Q_m, Q_{n-m}) \\ &\times d\Phi_m(Q_m; p_1, \dots, p_m) d\Phi_{n-m}(Q_{n-m}; p_{m+1}, \dots, p_n) . \end{aligned} \quad (18)$$

In order to combine the two sub-antennas to the required antenna structure, we have to take into account in the first decomposition a density that is proportional to

$$\frac{\Theta(\sqrt{s_n} - \sqrt{s_m} - \sqrt{s_{n-m}})}{(q_1 \cdot Q_m)(q_1 \cdot Q_{n-m})(q_2 \cdot Q_m)(q_2 \cdot Q_{n-m}) s_m s_{n-m}} . \quad (19)$$

2.2 Results

In this section, we present results obtained by **SARGE** and **HAAG**¹, the program that implements the hierarchical algorithm described before. In order to be as general as possible, the only cut we apply is

$$(p_i + p_j)^2 \geq s_0 , \quad (20)$$

where $i, j (i \neq j)$ runs from 1 to $n+2$ where n is the number of final-state particles. Unless explicitly mentioned differently, we use $s_0 = 900 \text{ GeV}^2$ and the total energy $\sqrt{s} = 1000 \text{ GeV}$. Moreover, all particles are assumed to be massless in order to compare with **SARGE**, with which only massless particles can be treated.

As it was mentioned in the introduction, we are interested in integrating sums of QCD antenna structures (2). We start by considering the simplest case, namely integrating the function

$$s^2 [(p_1 \cdot p_3)(p_3 \cdot p_4)(p_4 \cdot p_2)(p_2 \cdot p_5) \dots (p_{n+2} \cdot p_1)]^{-1} \quad (21)$$

that corresponds to a given permutation of the momenta, namely $(1, 3, 4, 2, 5, \dots, n+2)$. In Table 1 we give the results for **SARGE**, and **HAAG**. In all three codes the same single channel, corresponding to (21), has been used in the generation. N_{gen} and N_{acc} are the number of generated and accepted events, and by f we define

$$f = \frac{V_2}{I^2} , \quad (22)$$

¹HAAG stands for: Hierarchical AntennaA Generation.

where V_2 is the quadratic variance and I is the estimated integral. f is clearly a measure of the efficiency of the generator. Moreover ε , defined as

$$\varepsilon = \frac{\langle w \rangle}{w_{\max}}, \quad (23)$$

is the usual generation efficiency related for instance to ‘unweighted’ events in a realistic simulation. The results agree well, and exhibit the fact that the generated

jets	algorithm	N_{gen}	N_{acc}	I	ΔI	f	$\varepsilon(\%)$
4	SARGE	1×10^5	34853	$.251 \times 10^{-9}$	$.734 \times 10^{-11}$	85.9	0.34
	HAAG	5×10^4	31193	$.260 \times 10^{-9}$	$.280 \times 10^{-11}$	5.75	1.77
5	SARGE	2.5×10^5	30960	$.438 \times 10^{-10}$	$.153 \times 10^{-11}$	307	0.23
	HAAG	6.5×10^4	29855	$.442 \times 10^{-10}$	$.640 \times 10^{-12}$	13.6	1.02
6	SARGE	1×10^6	28383	$.487 \times 10^{-11}$	$.164 \times 10^{-12}$	1141	0.21
	HAAG	1.2×10^5	32070	$.487 \times 10^{-11}$	$.658 \times 10^{-13}$	21.9	1.48

Table 1: Results for the single-channel integration/generation.

densities of the generators the hierarchical type are much closer to the integrand. The same picture is reproduced for an arbitrary permutation.

For a realistic QCD calculation, the integrated function may be approximated by a sum over permutations. Therefore, an efficient generator has to include all possible channels, where each channel corresponds to a given permutation of the momenta. In that case, a multi-channeling optimization procedure can be applied, which is incorporated in **HAAG**. In order to study the efficiency of this optimization we consider the same integration as before, but with all channels contributing to the generation and allowing for optimization. In this optimization procedure, we discard channels that contribute less than a certain pre-determined fraction to the set of available channels. It is expected, of course, that in end the right permutation will be ‘chosen’ by the optimization. This is indeed the case and the results are presented in Table 2. We see that the optimization results to a picture close to the one obtained with the single channel generation, with some noticeable improvement in the case of **SARGE**.

jets	algorithm	N_{gen}	N_{acc}	I	ΔI	f	$\varepsilon(\%)$
4	SARGE	1×10^5	52516	$.262 \times 10^{-9}$	$.294 \times 10^{-11}$	12.6	1.29
	HAAG	5×10^4	34293	$.257 \times 10^{-9}$	$.210 \times 10^{-11}$	3.36	4.28
5	SARGE	2.5×10^5	32315	$.422 \times 10^{-10}$	$.106 \times 10^{-11}$	159	0.44
	HAAG	6.5×10^4	31063	$.444 \times 10^{-10}$	$.503 \times 10^{-12}$	8.32	1.17
6	SARGE	1×10^6	29138	$.476 \times 10^{-11}$	$.145 \times 10^{-12}$	933	0.45
	HAAG	1.2×10^5	33278	$.483 \times 10^{-11}$	$.595 \times 10^{-13}$	18.2	1.19

Table 2: Results for the all-channel generation with optimization.

As is the case for any multi-channel generator, a computational complexity problem arises when the number of channels increases. For instance, in our case we are facing a number of $\frac{1}{2}(n+1)!$ channels! On the other hand, it is also clear that the channels we are considering have a large overlap in most of the available phase space. It is therefore worth to investigate the dependence of the integration

efficiency on the number of channels used. This is presented in Table 3, where the full antenna

$$s^2 \sum_{P(2,\dots,n+2)} [(p_1 \cdot p_3)(p_3 \cdot p_4)(p_4 \cdot p_2)(p_2 \cdot p_5) \dots (p_{n+2} \cdot p_1)]^{-1} \quad (24)$$

is integrated, using a number of channels that has been selected on a random basis. We see the rather interesting phenomenon that a decent description can be achieved with a much smaller number of channels. Variations of this technique

# channels	2520	1500	1000	500	200	50	10
f	5.33	5.37	5.48	5.72	6.14	11.6	84.7
N_{acc}	26630	26521	26437	26676	27009	27190	27205
$\varepsilon(\%)$	11.2	13.1	11.6	7.1	7.5	1.7	0.28

Table 3: All-channel integration with subsets of channels for generation.

of using only subsets of channels, for example choosing another subset after each step of multi-channel optimization, lead to the same picture.

The complete results of the integration of the full antenna are presented in Table 4. We see that **HAAG** has a much better f factor than **SARGE**. On the other

jets	algorithm	N_{gen}	N_{acc}	I	ΔI	$\varepsilon(\%)$	f
4	SARGE	1×10^5	47483	$.166 \times 10^{-7}$	$.115 \times 10^{-9}$	4.21	4.8
	HAAG	6×10^4	42019	$.167 \times 10^{-7}$	$.810 \times 10^{-10}$	12.01	1.4
5	SARGE	3×10^5	39095	$.176 \times 10^{-7}$	$.162 \times 10^{-9}$	3.27	25.6
	HAAG	1.2×10^5	55234	$.177 \times 10^{-7}$	$.856 \times 10^{-10}$	7.53	2.7
6	SARGE	1.5×10^6	44529	$.157 \times 10^{-7}$	$.135 \times 10^{-9}$	2.95	109
	HAAG	1.8×10^5	47911	$.161 \times 10^{-7}$	$.905 \times 10^{-10}$	7.15	5.7
7	SARGE	1×10^7	47766	$.123 \times 10^{-7}$	$.988 \times 10^{-10}$	3.02	642
	HAAG	3.6×10^5	45599	$.123 \times 10^{-7}$	$.241 \times 10^{-10}$	5.11	13
8	SARGE	1×10^8	53560	$.784 \times 10^{-8}$	$.554 \times 10^{-10}$	3.29	4998
	HAAG	1×10^6	49206	$.789 \times 10^{-8}$	$.496 \times 10^{-10}$	6.30	39

Table 4: Results for the all-channel integration.

hand the ε exhibits a less dramatic effect. This is related to the fact that **SARGE** generates a phase space that is much larger than the one defined by the cut on s_0 . In that sense, if the main time consumption in a given computation is spent over the evaluation of the integrand (matrix element squared), it is more fair to compare the square of the estimated expected error, normalized by the number of accepted events N_{acc} . In that case we see that **HAAG** is still 2-3 times more efficient, and if we consider a smaller cut, namely $\sqrt{s_0} = 10$ GeV, this gain goes up to an order of magnitude (Table 5).

For a realistic calculation of the cross section of a QCD process, one may assume that the time it takes to perform one evaluation of the integrand is much larger than the time it takes to generate one accepted event and to calculate the weight. This means that the computing time is completely determined by the number of accepted events N_{acc} . We introduce

$$\frac{N_{\text{acc}} f}{N_{\text{gen}}} \quad (25)$$

jets	algorithm	N_{gen}	N_{acc}	I	ΔI	$\varepsilon(\%)$	f
4	SARGE	1×10^5	60986	$.364 \times 10^{-6}$	$.548 \times 10^{-8}$	0.631	22.7
	HAAG	6×10^4	46763	$.366 \times 10^{-6}$	$.235 \times 10^{-8}$	4.34	2.47
5	SARGE	2×10^5	43150	$.619 \times 10^{-6}$	$.165 \times 10^{-7}$	0.29	142
	HAAG	1×10^5	56034	$.643 \times 10^{-6}$	$.465 \times 10^{-8}$	1.84	5.23
6	SARGE	1×10^6	67811	$.114 \times 10^{-5}$	$.257 \times 10^{-7}$	0.28	502
	HAAG	1.4×10^5	51983	$.111 \times 10^{-5}$	$.883 \times 10^{-8}$	2.50	8.83
7	SARGE	5×10^6	84391	$.186 \times 10^{-5}$	$.346 \times 10^{-7}$	0.176	1723
	HAAG	2×10^5	44015	$.192 \times 10^{-5}$	$.177 \times 10^{-7}$	2.24	16
8	SARGE	5×10^7	175541	$.354 \times 10^{-5}$	$.517 \times 10^{-7}$.119	10618
	HAAG	5×10^5	58874	$.350 \times 10^{-5}$	$.289 \times 10^{-7}$	1.65	34

Table 5: Results for the all-channel integration with $s_0 = 100 \text{ GeV}^2$.

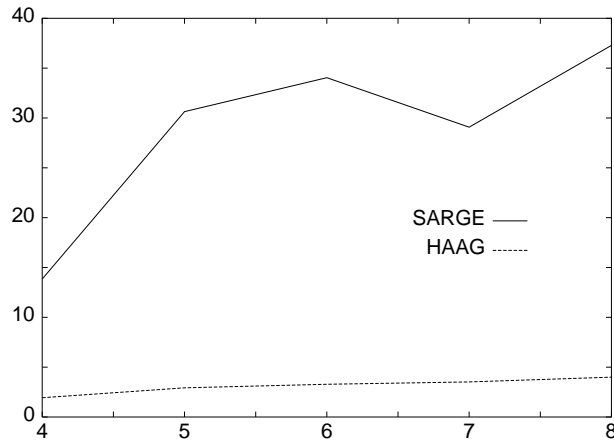


Figure 1: $N_{\text{acc}}f/N_{\text{gen}}$ (a measure of computing time) as function of the number of produced partons.

as a measure of the computing time. For a realistic calculation, one has to multiply this number by the evaluation time of the integrand, and divide by the square of the relative error one wants to reach. Fig.1 shows this quantity as function of the number of produced partons using the data of Table 5. According to this graph, a calculation with SARGE would take 10 times longer than the calculation with HAAG.

3 One-loop corrections to electroweak processes

Scattering amplitudes in Quantum Field Theory can be represented by Feynman diagrams whose number grows extremely rapidly (faster than factorially) in the number of loops and external legs. This places severe limits in the calculation of multi-particle scattering amplitudes. The last few years, the development of new innovative methods and algorithms made possible to overcome these limitations. Based on Schwinger-Dyson recursive equations the complete scattering amplitude is computed directly without recourse to explicit Feynman diagrams. This

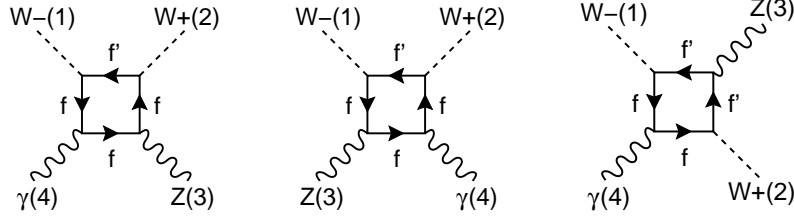


Figure 2: Three of the six 1PI diagrams that contribute to the fermionic one-loop correction of the $WWZ\gamma$ vertex. f represents a down-type fermion, and f' the corresponding up-type fermion. The other three diagrams are obtained by exchanging $f \leftrightarrow f'$ and taking the opposite fermion current.

results to a dramatic decrease in the computational cost which now depends only exponentially, *i.e.* $\sim 3^n$, in the number of external particles, n . Automatic computational tools, based on these Schwinger-Dyson recursive equations, have been developed that are able to describe any process within the Standard Electroweak theory and QCD [8, 9, 10, 11].

The high precision attainable by the future experiments calls for a reliable estimate of the higher order corrections to the multi-particle scattering processes. This means that the full one-loop contributions along with the higher order leading QED and electroweak corrections are necessary. Moreover, taking into account the unstable particle contributions, re-summed propagator corrections have to be included.

As a first step towards the extension of HELAC [8] towards the full one-loop level, re-summed boson propagators and fermion-loop corrections to boson vertices can be included. The main reasons to choose his collection of corrections is that it ensures gauge invariance [13], and that it is fairly straightforward to implement in an automatic program based on the Schwinger-Dyson method. If one, for example, wants to analyze processes that do not involve more than 6 fermions, the one-loop corrections do not involve diagrams with more than 4 external legs. So the “most complicated” diagrams that have to be included are 1PI fermion-one-loop four-point functions (Fig.2). Below, we give a sketch how to evaluate them in a straightforward manner. The lower-point functions can be evaluated analogously.

3.1 Evaluation of the one-loop four-point function

Each diagram represents a function of the masses m_i of the fermions, the momenta p_i of the vector bosons, their polarization vectors w_i and their couplings v_i, a_i to the fermion current. We conveniently choose to access them by permutating the

input of the general fermionic one-loop four-point function

$$\Gamma_4 = \int \frac{d^n q}{i\pi^2} \text{Tr}[P_1(q)V_1 P_2(q)V_2 P_3(q)V_3 P_4(q)V_4] \quad , \quad (26)$$

with ²

$$P_j(q) = \frac{\not{q} + \sum_{i=1}^{j-1} \not{p}_i + m_j}{(q + \sum_{i=1}^{j-1} p_i)^2 - m_j^2 + i\varepsilon} \quad \text{and} \quad V_j = \psi_j(v_j + a_j \gamma_5) \quad . \quad (27)$$

Possible divergences are treated within the formalism of dimensional regularization. Ambiguities regarding γ_5 are avoided if the vectors p_i and w_i are considered to be strictly 4-dimensional. The trace can be calculated with the help of computer algebra, for example with the program **FORM** [16], leading to

$$\Gamma_4 = \int \frac{d^n q}{i\pi^2} \frac{\text{num}_4(q; p_{1,2,3}, m_{1,2,3,4}, w_{1,2,3,4}, v_{1,2,3,4}, a_{1,2,3,4})}{\text{den}_4(q; p_{1,2,3}, m_{1,2,3,4})} \quad , \quad (28)$$

where the denominator function is defined by

$$\text{den}_l(q; p_{1,2,\dots,l-1}, m_{1,2,\dots,l}) = \prod_{j=1}^l \left[\left(q + \sum_{i=1}^{j-1} p_i \right)^2 - m_j^2 + i\varepsilon \right] \quad , \quad (29)$$

and the numerator num_4 is a fourth-order polynomial in the components of q . The integration problem is now reduced to that of the calculation of *tensor* integrals of the type

$$\mathcal{D}_{\nu_1 \dots \nu_r}(p_{1,2,3}; m_{1,2,3,4}) = \int \frac{d^n q}{i\pi^2} \frac{q_{\nu_1} \dots q_{\nu_r}}{\text{den}_4(q; p_{1,2,3}, m_{1,2,3,4})} \quad , \quad (30)$$

with $r = 0, 1, 2, 3, 4$. The Passarino-Veltman method [14, 15] uses the Lorentz covariance of these integrals to express them in terms of *coefficient functions* D through

$$\mathcal{D}_{\nu_1 \dots \nu_r}(p_{1,2,3}; m_{1,2,3,4}) = \sum_{i_1, \dots, i_r=0}^3 p_{i_1, \nu_1} \dots p_{i_r, \nu_r} D_{i_1 i_2 \dots i_r}(p_{1,2,3}; m_{1,2,3,4}) \quad , \quad (31)$$

with $D_{i_1 i_2 \dots i_r} = 0$ if an odd number of indices are equal to 0, and the interpretation

$$p_{0, \nu_1} p_{0, \nu_2} \dots p_{0, \nu_{2j}} \leftarrow g_{\{\nu_1 \nu_2} g_{\nu_3 \nu_4} \dots g_{\nu_{2j-1} \nu_{2j}}\} \quad . \quad (32)$$

The identification of the \mathcal{D} -functions and their expression in terms of the D -functions can also easily be performed by **FORM**. The output of **FORM** will contain symbols representing scalar products of the external momenta and the polarization vectors, contractions of these with the Levi-Civita symbol, and the D -functions. This output can easily be turned into a **FORTTRAN**-code. The scalar products and the Levi-Civita symbol are easy to be implemented, and the D -functions can be extracted from the **LoopTools**-package [17], or one can make the effort to extend the **FF**-package [18], upon which **LoopTools** is based.

²We define the sum $\sum_{i=1}^0 x_i$ as a sum of zero terms.

3.2 Result

We will present the result of an actual calculation now. For more results and more details about the program presented above, we refer to [20]. There, we will also digress more about the well-known problem that the Passarino-Veltman method to calculate tensor integrals is numerically unstable for certain values of the external momenta. It involves the inversion of a kinematic matrix, which can become singular, although the one-loop function is perfectly-well defined. One might hope that, in a Monte Carlo calculation of a cross section, the probability to get too close to these phase-space points is too small to be concerned about this problem. We experienced, that this hope may be trusted for cross section calculations concerning processes at the coming generation of accelerators if the computation of the coefficient functions is performed at quadrupole precision. Restricting the use of quadrupole precision like this, the cpu-time stays within acceptable limits. We calculated the total cross section for the process

$$e^- e^+ \rightarrow \mu^- \bar{\nu}_\mu u \bar{d} \tau^- \tau^+$$

using the following cuts: $E_l, E_q > 5\text{GeV}$ for lepton and quark energies, a maximal cosine of 0.985 between all (initial and final state) charged leptons and quarks, and $m_{ll}, m_{qq} > 10\text{GeV}$ for the invariant masses of charged leptons and quarks. We used the renormalization scheme of [19], and the following input parameters

$$\begin{aligned} m_W &= 80.35 \text{ GeV} & , & & m_Z &= 91.1867 \text{ GeV} \\ \text{Re}[\alpha^{(5)}(m_Z^2)^{-1}] &= 128.89 & , & & \alpha(0)^{-1} &= 137.03599976 \\ G_F &= 1.16639 \times 10^{-5} \text{ GeV} . \end{aligned} \quad (33)$$

As far as the tree-order cross section is concerned we use the widely used Fixed Width scheme, where a fixed W -boson width is implemented in all W -boson propagators and where the G_F -scheme is applied for evaluating the weak parameters. We recall that the latter is defined by using m_W , m_Z and G_F as input parameters, together with the two relations

$$s_W^2 = 1 - \frac{m_W^2}{m_Z^2} \quad , \quad \alpha = \frac{\sqrt{2}}{\pi} G_F m_W^2 s_W^2 \quad .$$

For the W and Z widths we use

$$\Gamma_W = 2.042\text{GeV} \quad , \quad \Gamma_Z = 2.49\text{GeV} \quad .$$

The results for $E = 500\text{GeV}$ are $\sigma_0/ab = 54.96(26)$ $\sigma_1/ab = 57.31(28)$, and the K-factor is $K/100 = 4.28(2)$. They show the expected contribution at the percent level of the higher order FL corrections to the total cross section. For comparison, the value of σ_0/ab computed with `0'Mega/WHIZARD` [11, 12] is given by 55.07(19).

4 Conclusions

We presented the algorithm **HAAG**, which uses the “hierarchical” strategy for phase space generation in order to efficiently map the antenna momentum structures, typically occurring in QCD amplitudes. It exhibits an improved efficiency compared to **SARGE** for multi-parton calculations, and it is more powerful in describing densities where a partial symmetrization over the permutation space is considered. Also, **HAAG** makes no fundamental distinction among massless and massive particles, so it can be used for an arbitrary multi-partonic process.

Furthermore we implemented one-loop corrections following the Fermion-Loop scheme in the program **HELAC** for automatic amplitude calculation and presented a result of a cross section calculation.

Acknowledgments

The authors would like to thank C. Schwinn for providing the result of the cross section calculation with **O’Mega/WHIZARD**. The research has been financially supported by the European Union under contract number HPRN-CT-2000-00149, and through a Marie Curie Fellowship under contract number HPMD-CT-2001-00105

References

- [1] W.J. Stirling *et al.*, Comp. Phys. Comm. **40** (1986) 359.
- [2] D. Bardin *et al.*, hep-ph/9709270.
- [3] C.G. Papadopoulos, Comp. Phys. Comm. **137** (2001) 247-254,
- [4] R. Kleiss and R. Pittau, Comp. Phys. Comm. **83** (1994) 141-146.
- [5] J.G.M. Kuijf, PhD thesis, University of Leiden, 1991.
- [6] P. Draggiotis *et al.*, Phys. Lett. **B483** (2000) 124-130,
A. van Hameren and R. Kleiss, Eur. Phys. J. **C17** (2000) 611-621,
- [7] A. van Hameren and C.G. Papadopoulos, Eur. Phys. J. **C25** (2002) 563-574,
- [8] A. Kanaki and C.G. Papadopoulos, Comp. Phys. Comm. **132** (2000) 306,
- [9] M. Mangano *et al.*, JHEP **0307** (2003) 001,
- [10] P.D. Draggiotis *et al.*, Eur. Phys. J. **C24** (2002) 447-458,

- [11] M. Moretti *et al.*, in *2nd ECFA/DESY Study 1998-2001*, no. LC-TOOL-2001-040, pp. 1981–2009, [hep-ph/0102195](#).
- [12] W. Kilian in *2nd ECFA/DESY Study 1998-2001*, no. LC-TOOL-2001-039, pp. 1924–1980.
- [13] W. Beenakker *et al.*, Nucl. Phys. **B500** (1997) 255-298,
- [14] G. Passarino and M.J.G. Veltman, Nucl. Phys. **B160** (1979) 151.
- [15] A. Denner, Fortsch. Phys. **41** (1993) 307-420.
- [16] J.A.M. Vermaseren, [math-ph/0010025](#), <http://www.nikhef.nl/~t68/>
- [17] T. Hahn and M. Perez-Victoria, Comp. Phys. Comm. **118** (1999) 153-165, <http://www.feynarts.de/looptools>
- [18] G.J. van Oldenborgh and J.A.M. Vermaseren, Z. f. Phys. **C46** (1990) 425, <http://www.xs4all.nl/~gjvo/FF.html>
- [19] W. Beenakker *et al.*, Nucl. Phys. **B667** (2003) 359-393,
- [20] A. van Hameren and C.G. Papadopoulos, in preparation.